Annual Review of Materials Research

Tailor-Made Additives for Melt-Grown Molecular Crystals: Why or Why Not?

Hengyu Zhou, Julia Sabino, Yongfan Yang, Michael D. Ward, Alexander G. Shtukenberg, and Bart Kahr

Department of Chemistry and the Molecular Design Institute, New York University, New York, NY, USA; email: mdw3@nyu.edu, as5243@nyu.edu, bk66@nyu.edu

Keywords

tailor-made additives, melt crystallization, spherulites, twisted crystals, chirality, polarity

Abstract

Tailor-made additives (TMAs) have found a role in crystal morphology engineering and control by specific binding to crystal surfaces through stereochemical recognition. The utility of TMAs, however, has been largely limited to crystal growth from solutions. In this review, we illustrate examples where TMAs have been used to influence the growth of crystals during cooling of their melts. In solution, the crystal growth driving force is governed by solute supersaturation, which corresponds to the deviation from equilibrium. In growth from melts, however, undercooling is the important thermodynamic parameter responsible for crystallization outcomes, a key difference that can influence the manner in which TMAs affect growth kinetics, crystal morphology, nucleation, enantioselective surface recognition, and the determination of the absolute sense of polar axes. When the crystallization driving force in a melt is small and diffusion is comparatively high, TMAs can exert their influence on well-faceted single crystals with the stereochemical richness observed in solution growth. Under high supercooling, where the driving force is large, ensembles of crystals can grow radially, masking stereochemical information and requiring new optical tools for understanding the influence of TMAs on emerging crystals.

1. PREAMBLE

1.1. Buckley

Impurities in a crystallization experiment—unintentionally present and usually unwanted—can affect outcomes such as crystal growth rates and morphologies, typically in unpredictable ways. In contrast, tailor-made additives (TMAs), also known as tailor-made auxiliaries, and admixtures (1)—crystal modifiers in abundance—can be intentionally introduced to influence crystallization in a more controlled manner. Buckley's monograph (2) reviewed work performed during the nineteenth century and the first half of the twentieth century related to the effects of imperfect media on crystal growth. A more contemporary perspective was provided by Sangwal (3). Buckley performed countless experiments with commercial dyes (4)—among other additives—in which he aspired to place the effects of habit modification on a structural and stereochemical basis. This heroic work unfortunately was for naught because commercial dyes are often adulterated with impurities. Many dyes, for example, are mixtures of stereo- and regioisomers, while tautomeric and acid-base equilibria abound. Moreover, in the 1930s, when Buckley did most of the experiments (5–7), organic stereochemical analysis was still underdeveloped. Buckley's data were adulterated, and he did not have the structural underpinnings to make sense of them even though his chemistry was well conceived (8). Similar analyses were performed contemporaneously (9) but were likewise based on a premature structural foundation (10). Only in the 1990s did single-crystal spectroscopies directed at dyed crystals begin to unravel the supramolecular stereochemistry underlying the interactions of dyes with crystals (9–18).

1.2. Bernauer

Buckley's experiments in Manchester were directed at the modification of simple salts from aqueous solutions (**Figure 1a**). Just a few years earlier, Bernauer (19, 20) in Berlin studied the effects of additives on crystal growth, but on crystals grown from melts. Besides the difference between solution and melt growth, there were two other important distinctions between the works of Buckley and Bernauer: (*a*) whereas Buckley used impure synthetic dyes as additives, Bernauer used natural resins, complex mixtures of organic compounds produced by plants for which the compositions also were largely unknown; and (*b*) Buckley measured the relative areas of faces expressed by single crystals, whereas Bernauer interpreted the optical textures, between crossed polarizers, associated with morphological changes in ensembles of crystals.

A typical consequence of resin additives can be illustrated by a dramatic transformation of the texture of recrystallized aspirin in the presence of Canada balsam, the sap from the *Abies balsamea* fir tree (**Figure 1b,c**). Broad blades are transformed into tightly packed, radially arranged fibrils that show an optical rhythm along their lengths that was correctly interpreted (21, 22) as a consequence of the precession of the refractivity resulting from crystals twisting in phase on the mesoscale, a stunning example of spontaneous pattern formation (23). The crystals organized themselves as so-called banded spherulites, radial aggregates of fine lamellae with concentric bands of optical contrast along the radii, which are telltale evidence of twisting. It was claimed (20, 24) that approximately one-quarter of molecular crystals can be made to grow with this texture from the melt. We have found that the figure may be closer to one-third (25, 26) for randomly selected compounds or even one-half in some classes of compounds (27).

Bernauer summarized his research in a book titled "*Gedrillte" Kristalle* (20). "*Gedrillte*" is printed between quotation marks, most likely suggesting "like a drill" or "twisted," but also perhaps invoking the notion of in-phase behavior or soldiers marching as in a military drill. The chief results were presaged in an earlier report (19). He described 135 simple molecular crystalline substances that ostensibly twisted around their axes of growth during cooling of their melts in thin-film
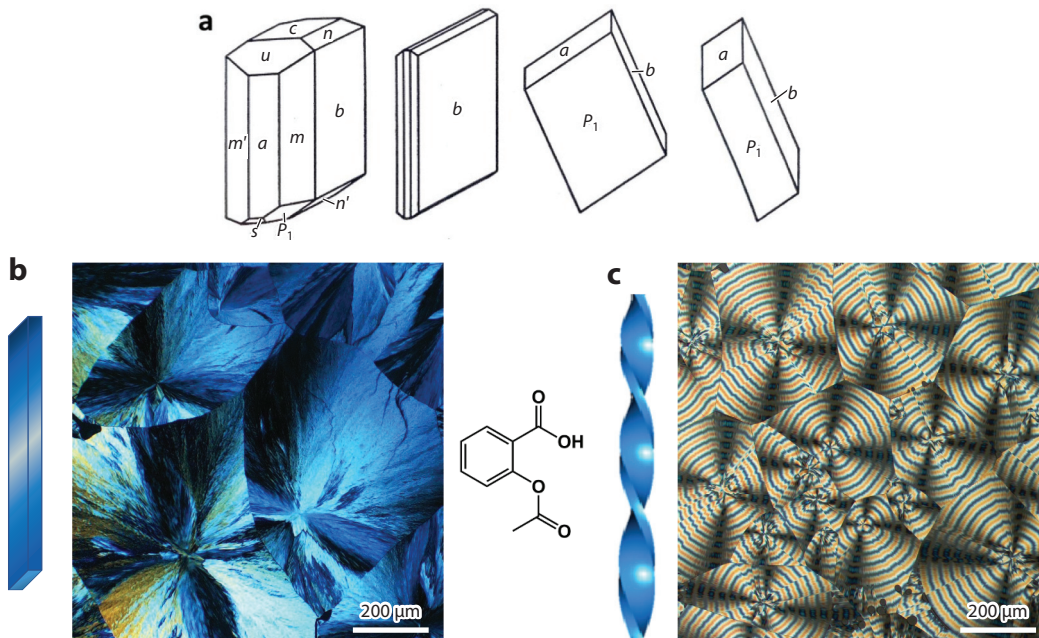
Figure 1

(*a*) Drawings of $K_2Cr_2O_7$ single crystals from aqueous solutions with habits modified by sundry synthetic dye additives. Distinct letter labels indicate symmetry-independent faces according to standard conventions for crystals. Panel adapted from Reference 2. (*b*) Broad blades of aspirin (with the structure shown) grown from the melt at room temperature. (*c*) Twisted aspirin grown from the melt with 15 wt% Canada balsam, following the method in Reference 19, at room temperature.

form. The resin additives probably increased the melt viscosities, which is consequential (see Section 2.2). This was before the age of synthetic polymers, which themselves were discovered in the 1950s to frequently form ring-banded spherulites (28, 29).

Bernauer measured half pitches—the distances between two adjacent bands with equivalent interference colors—to assay twisting in crystals grown from melts. Twist intensity (*i*) was scored as 1, 2, or 3 depending on whether the number of half rotations per millimeter was 0–2, 2–10, or 10–20, respectively. Bernauer also scored the areal fractions (*f*) of twisted crystals as I, II, or III, corresponding to 2–20%, 20–50%, or 50–100%, respectively. Incomplete coverage could be a result of the concurrent growth of twisted and untwisted polymorphs or inhomogeneous distributions of the resins. The first ten compounds of the large data table are provided in **Figure 2** with their corresponding English names in the figure caption. Most of these compounds have been regrown in our laboratory. Chalcedony is a mineral not subject to experiment, and cocaine hydrochloride was not evaluated for obvious reasons.

The general roles of additives in the melt were to increase viscosity, suppress diffusion, slow nucleation, and inhibit crystallization until larger undercoolings and higher crystallization driving forces can be achieved. This often leads to finer crystals with more extreme aspect ratios that are more likely to twist by whatever mechanism (21, 25). The elastic energy to twist a fibril is roughly proportional to the inverse fourth power of the radial cross section (30, 31). The influence is not chemically specific but rather is a consequence of changing the dynamics of the aggregate medium (32). One would not, or could not, say that these resins were being used as TMAs. Given the complexity of his natural resins, Bernauer may have been using TMAs in some cases, but only in hindsight and not deliberately.

						rein[4]		Can.		Col.		Sand.		Bak.		Koll.		
Nr.	Name	Formel	Symmetrie	Smp. Grad	Lit.	i	f	i	f	i	f	i	f	i	f	i	f	Anmerkungen
1	Triphenylthienylblei	Pb(C₆H₅)₃·C₄H₃S	tetragonal[2]	~150	—	—	—	2—3	Sp.	3	I	3	I	1—3	II	3	I	
2	Harnstoff	CO(NH₂)₂	tetr.-skal.	132	III, 539	—			Tr.	1	III	1—2	I	1—2	III	2	Sp.	
3	Chalcedon	SiO₂	trig.-trap.	—	—	1—2	III											
4	Benzil	C₆H₅·CO·CO·C₆H₅	„	95	V, 200	—		—		2—3	I			2—3	Sp.	—		Rizinusöl 1 II
5	Itaconsäure	COOH·C:CH₂·CH₂·COOH	rhomb.-bipyr.	161	III, 418	2—3	III	1—2	I	1	I	1	I	1	I	1	II	
6	Resorcin[1]	C₆H₄(OH)₂	rhomb.-pyr.	110	IV, 85	—		1	I	3	II	2	II	1	I			Cedernöl 1 Sp., Rizinusöl 1 Sp.
7	Hippursäure	C₆H₅·CO·NH(CH₂·COOH)	rh.-bisphen.	188	IV, 531	2	II	2	II	2	II	2	II	2	II	2	II	
8	Santonin[2]	C₁₅H₁₈O₃	„	170	V, 461	2—3	III	1—2	III	1	III	1	III	1—3	III	1	III	
9	Cocainchlorhydrat	C₁₇H₂₁O₄N·HCl	„	182	V, 888	3	II			2—3	II	2—3	III	3	III	1	III	
10	Methylharnstoff	CO·NH₂·NH(CH₃)	„	102	III, 550	2	I	2—3	II	2—3	III	3	III	2	I	1	III	

Tabelle IIa
Verzeichnis der untersuchten gedrillten Kristallarten. 1. Symmetrie bekannt

Figure 2

The first 10 entries of Table IIa in "*Gedrillte" Kristalle* (20), "List of twisted crystals examined. 1. Of known symmetry." The corresponding English names for the compounds in the second column are (1) triphenythienyl lead, (2) urea, (3) chalcedon (a fibrous form of quartz), (4) benzil, (5) itaconic acid, (6) resorcinol, (7) hippuric acid, (8) santonin, (9) cocaine hydrochloride, and (10) methyl urea. The third column contains the formula (*Formel*), the fourth column the symmetry (*Symmetrie*), the fifth column the melting points (*Smp. Grad*), and the sixth column literature citations (*Lit.*). The next six columns describe the outcomes (twist intensity, *i*, and areal fraction, *f*) of growth under different conditions: pure (*rein*) or in the presence of Canada balsam resin (*Can.*), colofonium or rosin (*Col.*), sandarac (*Sand.*), Bakelite (*Bak.*), and collolite with dammar resin and paraffin oil as the essential components (*Koll.*). Finally, some notes (*Anmerkungen*) are offered for the odd experiment with castor oil (*rizinusöl*) or cedar oil (*cedernöl*). Figure reproduced from Reference 20.

TMAs have traditionally been studied in solution crystal growth experiments. We introduced above a pair of pioneers who might have experienced the effects of TMAs on crystal growth, with one focused on solution growth and the other on melt growth, each beset with problems of purity. This established a parallelism that has not been maintained in subsequent generations of crystal growers. In Section 2.1, we present an example from our laboratories of the use of TMAs in solution growth to illustrate chemical strategies for modulating crystal growth through the judicious choice of additives. In Section 2.2, we discuss differences between solution growth and melt growth and possible explanations for why TMAs in melt growth have been understudied while illustrating points of connection between solutions and melts, particularly near equilibrium. We then summarize our attempts to explore whether Bernauer, in his many hundreds of crystallization experiments from the melt, was exercising the influence of TMAs.

2. PRINCIPLES OF TAILOR-MADE ADDITIVES

2.1. Tailor-Made Additives: An Example of Solution Growth

The equilibrium shape of a crystal can be predicted, in principle, from idealized surface structures and energies, but shapes of real crystals are subject to gradients in nutrients and temperature as well as the influence of adventitious impurities in the growth medium (33–38). So-called TMAs are deliberate impurities introduced to test hypotheses of crystal growth mechanisms and ultimately direct growth (39). TMAs have been used to resolve conglomerates (40, 41), to assign absolute configurations (42, 43), and to control nucleation (43, 44), growth rates (44, 45), and morphologies (45, 46). TMAs are particularly instructive when they make stereochemistry vivid by changing the shape of a crystal predictively (47). TMAs have been used almost exclusively in solution growth. Therefore, in order to give a clear illustration of their use and the judgments derived from them, an example of the application of TMAs in solution growth is introduced here.

As a part of developing a new therapy for ʟ-cystine kidney stones, we designed TMAs and studied their effects on the crystallization of ʟ-cystine from solutions (48–51). A series of ʟ-cystine derivatives was prepared (50, 52). The effects of small (<0.1 mM) concentrations of these
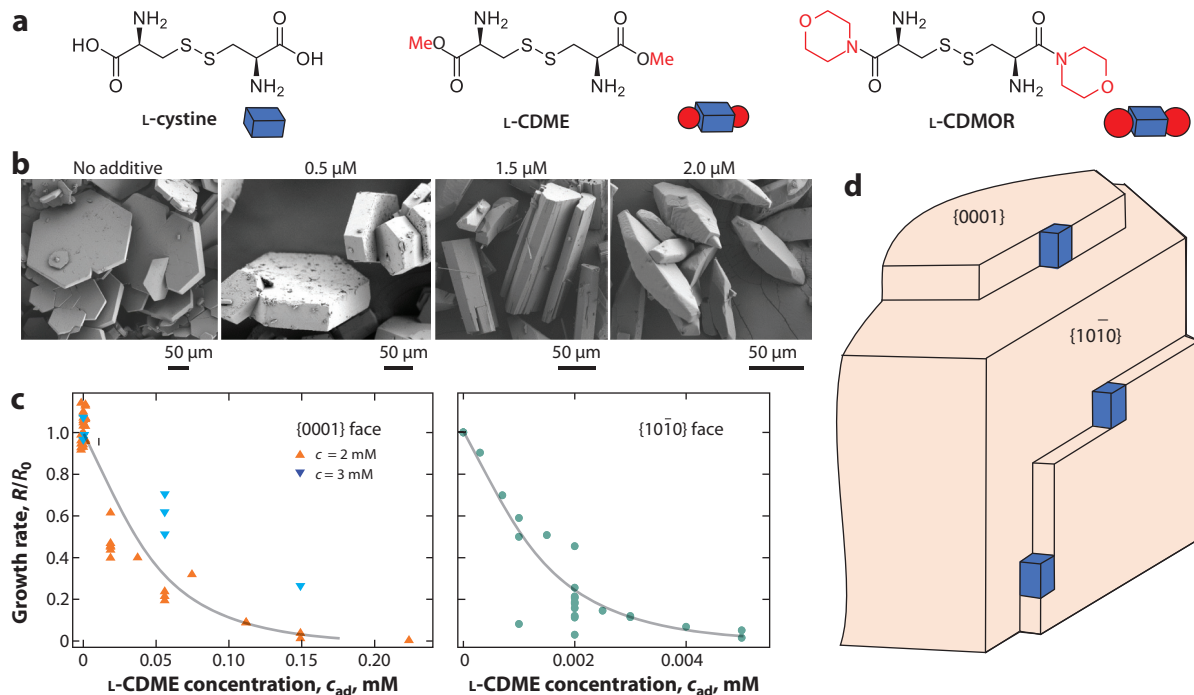
Figure 3

Growth manipulation of hexagonal L-cystine crystals with TMAs. (*a*) Molecular structures of L-cystine and two TMAs prepared by replacing both hydroxyl hydrogens with either methyl or morpholine groups. Diagrams illustrate modifications of the L-cystine molecular shape. (*b*) Scanning electron micrographs depicting morphology evolution of L-cystine crystals grown in the presence of L-CDMOR. As the concentration of TMA increases, thin hexagonal plates are replaced by thicker plates and rod-like crystals. Eventually the hexagonal polymorph of L-cystine is replaced by the tetragonal polymorph. (*c*) Growth rates of L-cystine in the presence of L-CDME normalized to the growth rate without additives, R/R_0, on {0001} and {10$\bar{1}$0} faces. Note that the scale for the additive concentration, c_{ad}, is very different in the two graphs, and the same growth inhibition of the {0001} face requires a much higher level of L-CDME than of the {10$\bar{1}$0} face. The L-cystine concentration is 2–3 mM. (*d*) Schematic representation of an L-cystine crystal showing kink sites where incorporation of L-cystine molecules takes place. Blue blocks signify L-cystine molecules in the kink. Kink sites on the {10$\bar{1}$0} face can more easily accommodate bulkier TMA molecules compared with more constrained kink sites on the {0001} face, leading to preferential adsorption on and inhibition of {10$\bar{1}$0} faces. Abbreviations: CDME, cystine dimethyl ester; CDMOR, cystine dimorpholide; TMA, tailor-made additive. Figure adapted with permission from Reference 51.

inhibitors on the crystallization of L-cystine from supersaturated aqueous solutions (concentration of 1–3 mM) were tested. The best inhibitors turned out to be several L-cystine diesters and diamides (two examples are shown in **Figure 3a**), performance that can be attributed to their role as "molecular imposters," wherein the central portion of the inhibitors binds to crystal binding sites through stereochemical recognition. In the presence of these TMAs, crystal morphology changed from thin hexagonal plates to rod-like crystals, and at higher additive concentrations, the hexagonal polymorph of L-cystine stopped crystallizing and a tetragonal polymorph formed instead (**Figure 3b**). Real-time, in situ atomic force microscopy measurements and ex situ morphology observations demonstrated that growth rates of both {0001} and {10$\bar{1}$0} faces decreased as concentrations of the additives increased, approaching zero above critical concentrations. The growth of the {10$\bar{1}$0} face was inhibited substantially more than that of the {0001} face, explaining the observed morphological changes (**Figure 3c**). These observations can be rationalized by considering kink sites on the surface of L-cystine crystals, where the molecules attach to the surface

(**Figure 3d**). On the {10$\bar{1}$0} faces, attachment to kinks does not require much additional space to accommodate the bulky end groups of TMAs, depicted by orange circles in **Figure 3a**. As a result, the distribution coefficient of additives is close to one. Incorporated additives, however, disrupt crystallization of the next L-cystine layer. On the {0001} faces, kink sites are more geometrically constrained and incorporation of TMAs requires significant distortion of the molecule, reducing the distribution coefficient by a factor of ~50. Consequently, inhibition of this face requires much higher TMA concentration in solution. The mechanism of stereochemical control outlined here was supported by corroborating growth kinetics, crystal optical data, and calculation of TMA binding energies into kink sites on both growth faces (49, 50). Alternatively, adsorption onto one of the sites along the large riser (six molecules high) could block the growth of the next layer, resulting in the same overall effect.

2.2. Solution Versus Melt Growth

Most experiments with TMAs involve crystals at ambient conditions from low concentration (molar fraction of solute rarely exceeding 0.01) aqueous or organic solutions. The driving force for crystallization from solution is $\Delta\mu = RT\ln(\frac{c}{c_{eq}})$ at constant temperature, where c is the concentration, c_{eq} is the concentration at equilibrium, and R is the gas constant (38). The driving force is typically small such that crystals have polygonal shapes and grow by screw dislocation or two-dimensional nucleation mechanisms on atomically flat surfaces (38).

The driving force for crystallization from the melt or supersaturation can be defined as $\Delta\mu = \Delta H_f \Delta T / T_m$, where ΔH_f is the enthalpy of fusion, T_m is the equilibrium temperature, and ΔT is the undercooling ($T_m - T$). Molecular crystals growing from the melt at small driving force (supercoolings < 10–20°C) are also polygonal and grow by the same mechanisms as crystals growing from solutions (53). The absolute growth rates from the melt are often significantly higher than growth rates from solution at the same driving force due to the much higher concentration of material in the melt (the molar fraction is close to one). Combined with slower diffusion in the melt, this may result in accumulation of TMAs at the growth front, increasing incorporation of additives with stronger effects on the crystal morphology. On the other hand, compared with crystallization from solution, the absolute temperature for crystallization from the melt is usually higher, resulting in faster desorption of molecules to kinks and thus better discrimination between host and guest, reducing TMA influences.

Unlike most solution experiments, crystallization from the melt often can be performed at high crystallization driving forces (supercoolings of hundreds of degrees Celsius), where crystals acquire needle-like habits, exhibit high degrees of branching, and form spherulites (54). The growth mechanism under these kinetic conditions involves attachment to highly kinked surfaces at the crystal tips (55–57). Rough features conspire against stereoselective processes (58) such that TMA binding to crystal faces can become indiscriminate. Spherulites grow from very viscous melts—sometimes even from glasses—that prevent significant material redistribution, assuring high concentrations of TMAs at the growth front. Diffusion is inversely related to viscosity in the Stokes–Einstein equation. During crystal growth from solution, solvent viscosity can vary by an order of magnitude (from 0.3 cP for acetone to 3 cP for 1-butanol at room temperature), while melt viscosities can vary by factors of billions (32). For example, the viscosity of abietic acid, a resinous acid found in Canada balsam, is 200 cP at 130°C and can be as large as 7×10^{13} cP when glassy at room temperature (59). Such large differences in viscosity can change one growth mechanism into another where TMAs are no longer consequential (34), or they can force a TMA that is indifferent in solution to exert an influence in the glassy state because it has no better choice. Massive accumulation of additives at the growth front, however, can be precluded by deposition of additives in

the space between spherulite fibers. The mechanisms of additive action on rough surfaces are not well studied, but one can reasonably expect that cooperative inhibitory effects of TMAs through the Cabrera–Vermilyea step pinning mechanism (60) should be reduced, thereby mitigating the effect of high additive concentration at the growth front. In summary, crystallization from melts exhibits features that can either enhance or mitigate the effects of TMAs compared with crystallization from solution. The similarities and differences are not known and require investigation (61).

There is no more common example of crystallization from melts on Earth than the freezing of water. Ice inhibition with additives is a major field of research. Polar organisms are reliant on stereoregular additives in the form of ice-inhibition proteins to survive (62, 63). The food industry is likewise reliant on additives to prevent the crystallization of many frozen products (64, 65). We do not discuss ice crystallization with stereospecific additives here, as it is the subject of many previous reviews (e.g., 66, 67).

2.3. Additives in Melt Growth

In melts, the crystallization temperature is the most important growth variable in the absence of additives, and its effects are compounded with the kinetic influence of additives. We present a case where crystals grow with TMAs from the melt at low driving force and then discuss a common scenario at high driving force to introduce the next section.

2.3.1. Low driving force. *meta*-Chloronitrobenzene (*m*-CNB), prized for its nonlinear optical response (68), forms well-faceted crystals from the melt at small undercoolings. *m*-CNB crystallizes in the polar space group $Pbn2_1$, with $Z = 4$. Melt-grown crystals are bounded by {020}, {120}, {021}, and {101} facets (**Figure 4b,c**). Crystals grown from the acetone solution were comparable to the melt-grown crystals, although with additional {110} facets (69, 70). The crystals are polar, but the sense of the polar axis is evident neither in melt-grown crystals (**Figure 4c**) nor in
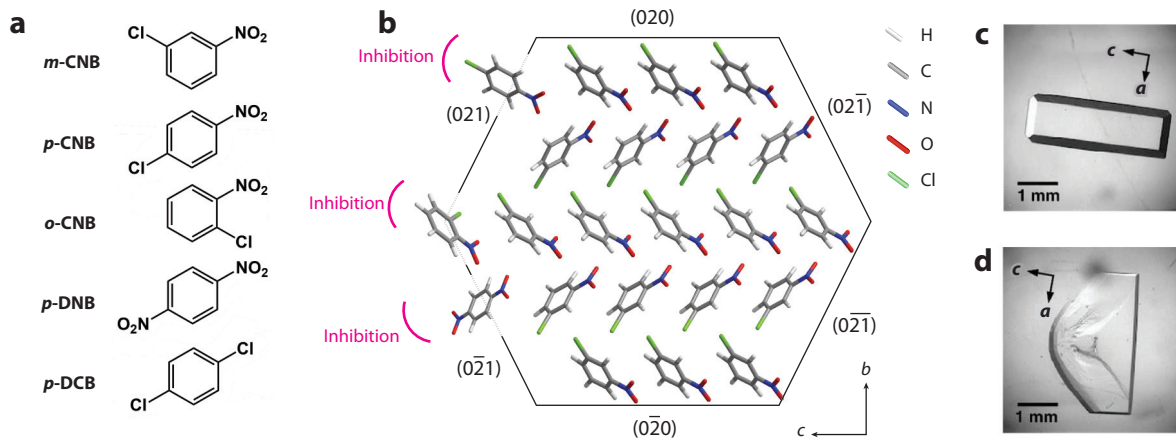

Figure 4

Growth modification of *m*-CNB with TMAs. (*a*) Molecular structures of *m*-CNB and its TMAs: *p*-CNB, *o*-CNB, *p*-DNB, and *p*-DCB. (*b*) Schematic diagram showing the arrangement of *m*-CNB molecules viewed along the *a*-axis of the crystal, space group $Pbn2_1$. Inhibition by different TMAs is also shown. (*c*) Pure *m*-CNB single crystal grown from the melt. (*d*) *m*-CNB grown from the melt with 13.0 wt% *p*-CNB. Abbreviations: *m*-CNB, *meta*-chloronitrobenzene; *o*-CNB, *ortho*-chloronitrobenzene; *p*-CNB, *para*-chloronitrobenzene; *p*-DCB, *para*-dichlorobenzene; *p*-DNB, *para*-dinitrobenzene; TMA, tailor-made additive. Panels *c* and *d* reproduced with permission from Reference 74.

solution-grown crystals. The nitro groups of *m*-CNB protrude from surfaces oriented toward −*c*, whereas the nitro groups are oriented to the interior of the crystal on the opposite side. Thus, TMAs with nitro groups are well disposed to differentiate between the ends of *m*-CNB crystals under the presumption of nitro group–nitro group superposition of TMAs and host molecules. In this way, depending on the differential modification of the ends of the polar axis, the sense of polarity was assigned and compared for crystals grown from solutions and melts (71). Accordingly, growth of *m*-CNB from its melt with TMAs has been a focus of research in the past 30 years (72–75). The addition of either *para*-chloronitrobenzene (*p*-CNB) or *para*-dinitrobenzene (*p*-DNB) modified the morphology of crystals grown near the melting point. Minor {101} facets appeared with 1 mol% of the TMAs. With 5 mol% (72) or 13 wt% (74), one end of the <001> growth direction became rounded, yielding a strongly modified polar form (**Figure 4d**). The thickness of the crystal along the <010> direction was reduced at the same time due to TMA inhibition on {021} facets. Similar modifications were observed with 25–35 mol% of *ortho*-chloronitrobenzene (*o*-CNB).

Force-field computations (76) were performed to assess the attachment energies of TMAs on *m*-CNB surfaces and compare them to experimentally measured growth kinetics. The binding energy difference, ΔE_B, the energy of exchanging a TMA with a host molecule on a surface, was highly site specific. The lowest values were observed when the additive molecules adopted an orientation where the nitro groups of additives were coincident with those of the host molecules. Attachment energies, E_{att}, were also calculated for TMAs in crystal slices or surfaces. The calculations revealed that *o*-CNB, *p*-CNB, and *p*-DNB were most likely to become incorporated into the crystal through the chlorine-rich end of the polar axis, directed by their nitro groups. Thus, the chlorine-rich end of the {021} and {101} faces would be more affected by inclusion of these TMAs, whereas the nitrogen-rich end would be barely affected. This proposition is also corroborated by the absence of an effect on crystal morphology by *para*-dichlorobenzene, which lacks nitro groups.

Growth kinetics measured for *m*-CNB growth from a melt containing *p*-CNB additives revealed a power law relationship that describes the growth rate of each facet as $V = K_v \sigma^g$, where K_v is the growth rate coefficient, the exponent g is the order of the growth process, and σ is the supersaturation related to $\Delta\mu$ given previously by $\sigma = \Delta\mu/RT$. The experimental power laws that describe the growth rate (*m/s*) of *m*-CNB with 25 mol% *p*-CNB from the melt on two ends of the polar axis of *m*-CNB were reported as $1.7 \times 10^{-4}\sigma^{1.8}$ for the nitro-rich end and $7.5 \times 10^{-6}\sigma^{1.4}$ for the opposing end, assuming that K_v is temperature independent over small undercoolings. These results indicate that the surfaces terminated with chloro groups are more inhibited by the TMAs than the surfaces terminated with nitro groups, consistent with attachment energy calculations.

2.3.2. High driving force.

Under high driving forces in supercooled melts, a nucleus often becomes unstable and undergoes small-angle branching. As one growth direction is usually fastest, branching is also fastest in the perpendicular direction, leading to the so-called sheaf-of-wheat morphologies that ultimately evolve into spherulites (54, 77). Under these circumstances, all spherulites are radial anisotropic bodies of one of two types, positive or negative, with the larger refractive index in the radial or tangential direction, respectively. Otherwise, they are stereochemically silent objects. Sometimes discrete eyes can be seen near the nucleus that are connected by a line orthogonal to the protogenic crystal, but often the eyes cannot be resolved because the nucleus region is chaotic (54). Ring-banded spherulites, endowed with twisting radii, often induced by additives. This can be a rich playground for exploring the role of TMAs in stereochemistry.
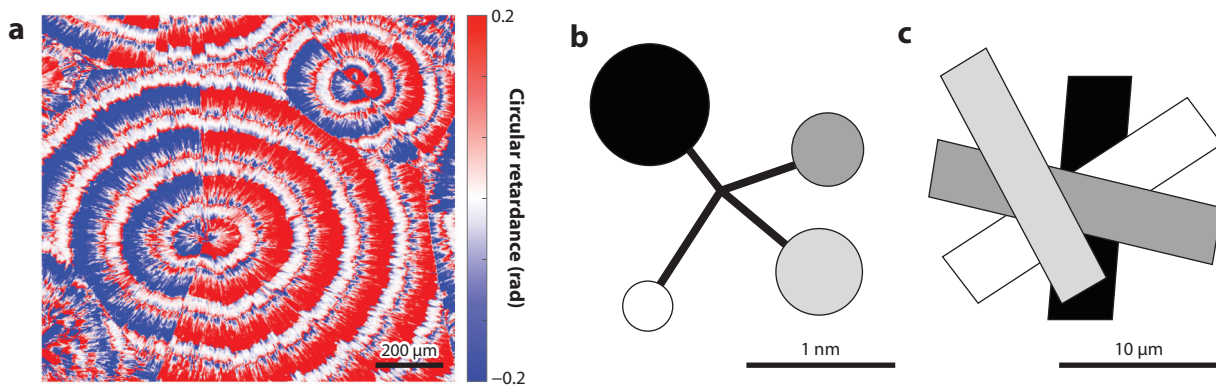
Figure 5

Optical activities. (*a*) Circular retardance micrograph of aspirin crystallized from the melt determined by Mueller matrix imaging microscopy. (*b*) Classical optical activity arises through the induced dipole–induced dipole interactions of groups of different polarizabilities, dissymmetrically oriented as in the tetrahedral compound schematically illustrated here, in which the circles represent different atoms or groups of atoms. (*c*) A mesoscale distribution of anisotropic crystallites can result in differential refraction of left and right circularly polarized light, an effect that depends on only the dielectric susceptibility tensor and not the magnetoelectric tensor. This characteristic is electric dipole-allowed and therefore can be comparatively large. The shades of gray in panel *b* represent different atoms or groups of atoms, while in panel *c* they represent different crystal orientations.

3. INFLUENCE OF ADDITIVES ON TWISTED CRYSTALS

3.1. Mesoscale Polarimetry

The assignment of absolute mesoscale stereochemistry requires a device for assigning the sense of twist and/or splay in a banded spherulite. The analysis of the differential transmission of left and right circularly polarized light in highly structured polycrystalline materials can provide information about stereochemistry on the mesoscale directly. The circular birefringence, usually presented phenomenologically as circular retardance (CR), measured in these instances does not arise from natural optical activity, a consequence of the dissymmetry of polarizable groups within a molecule (78) or a single crystal (79). Rather, it stems from the dissymmetry of anisotropic crystallites with respect to one another (**Figure 5**) (80–87).

As polarized light traverses a homogeneous medium, its state undergoes a continuous evolution, which can be accounted for in terms of the elementary linear optical properties of the medium (88, 89). Under circumstances in which light may pass from one anisotropic crystal to the next, effects may arise that depend on the disposition of the component crystals with respect to one another. Materials that are composed of anisotropic crystallites with only linear retardance [$\mathrm{LR} = (2\pi(n_0 - n_{90})L)/\lambda$] can by superposition behave as if they are optically active with a sense of rotation or CR [$\mathrm{CR} = (2\pi(n_L - n_R)L)/\lambda$], where n_0 and n_{90} are refractive indices for orthogonal polarizations and n_L and n_R are refractive indices for left and right circularly polarized light, respectively.

We measured the linear optical properties of our melt-grown spherulites with customized, home-built Mueller matrix imaging microscopes (90–92). Frequently, the CR was much larger than could be expected from the natural optical activity of molecular single crystals (93). Mechanisms for optical activity based on multilayered anisotropic structures do not rely on light–matter interactions beyond the electric dipole approximation. Such effects can be quite large and comparatively easy to measure.

To confirm that CR images arose from the superimposition of overlapping anisotropic lamellae misoriented along the light path, we multiplied Mueller matrices (M_k, $k = 1, 2, \ldots, N$), each with

a fraction of the overall LR, LR/N, albeit with each layer progressively rotated in the same sense by a small angle $\varphi/(N-1)$ using the rotation matrix $M_{\text{rot}(k)}$ as follows: $M_k = M_{\text{rot}(k)}^{-1} M_1 \, M_{\text{rot}(k)}$, $k = 2, 3, \ldots, N$. A product of Mueller matrices describes the optical response of an ensemble of N progressively misoriented lamellae, $M_{\text{total}} = \prod_{k=1}^{N} M_k$. In this way, CR was shown to arise in the twist and splay of anisotropic lamellae even in the absence of any molecular chirality.

A vivid example mapping the sense of splay of anisotropic lamellae in spherulites of polycrystalline aspirin grown from the melt is shown in **Figure 5a**. CR is nonzero even though aspirin is centrosymmetric and cannot have natural optical activity. The etiology of the sensitivity to circularly polarized light arises in the bisection of a spherulite into halves that are dextrorotatory and levorotatory. Aspirin lamellae splay by small-angle branching of a nucleus with $2/m$ (C_{2h}) symmetry with a positive sense (right-handed) for one ⟨010⟩ direction and a negative sense for the opposite. This is an example of an enantiopolar spherulite, the detection of which is owed to the CR anisotropy that would otherwise remain hidden.

3.2. Case Studies

In this section, we present two cases where we applied TMAs to help determine the absolute growth direction of the twisted crystals grown from the melt. Then we present a new study applying TMAs to break the heterochirality of the banded spherulites and to help assign absolute growth direction for centrosymmetric crystals.

3.2.1. Resorcinol. Resorcinol (**Figure 6a**, *top*) is a prosaic compound that flows into this review from two discrete streams. First, Wallerant (94), a mineralogist, was frustrated that Pasteur's sodium ammonium tartrate was the singular example of molecular dissymmetry manifest in crystal form. He looked for others by using tartaric acid molecules to induce dissymmetry in molecular crystals of other substances. In this way, he prepared, among other compounds, banded spherulites composed of twisted crystals of resorcinol grown from the melt that twisted stereospecifically in
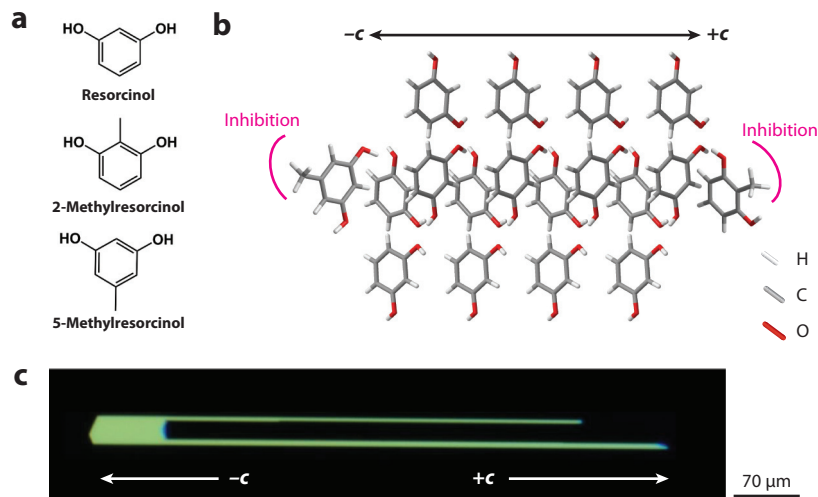

Figure 6

(*a*) Chemical structures of resorcinol and its tailor-made additives, 2-methylresorcinol and orcinol (5-methylresorcinol). (*b*) Schematic illustration of methylresorcinols acting as inhibitors on *c*-axes of a resorcinol crystal. (*c*) Polarized light microscopy images of β-resorcinol single crystals grown with 5 wt% orcinol at supercooling of 0.5°C.

accord with the configuration of the additive involved. We reproduced this useful model. The sense of helical twisting was established as originally described by Wallerant by following the movement of the extinction bands in the petrographic microscope, marking optic axes outcrops while rotating the spherulites about their radii (95). A clockwise twist, looking in the direction of growth as well as down upon the sample, drives the bands along the growth direction if the helix is left-handed. A second polymorph, also twisted, behaved in reverse. These two phases were not the α and β phases, the first polymorphs of a molecular crystal to be determined by X-ray crystallography (96–98). In the fullness of time, one of the phases was shown to be new and was dubbed ε (99). Phases α and β are easily obtained from solution, whereas from melts, β and ε are favored.

Second, resorcinol arguably has been the most frequent target of TMAs from solution ever since Wells (100) pointed out that one end of the polar axis of the α form grows more rapidly than the other. Which is faster, and for what reason? Many have contributed experiments, speculations, and computations aimed at answering this question. We have summarized these developments at length (99). We aimed to examine the underexplored realm of melt growth using TMAs, which necessarily implied studying the β and ε forms since the α form does not grow from the melt. β-Resorcinol adopts the same polar space group $Pna2_1$ as the α form. It was shown that pyrogallol [$1,2,3$-$(OH)_3C_6H_3$] stereoselectively inhibited oxygen-rich $\{01\bar{1}\}$ facets of α-resorcinol while phloroglucinol [$1,3,5$-$(OH)_3C_6H_3$] and orcinol [$1,3$-$(OH)_2$–5-$CH_3C_6H_3$] inhibited hydrogen-rich $\{011\}$ facets (101–103). Inspired by this previous work on α-resorcinol, we selected a similar set of TMAs to study the absolute sense of the growth direction of β-resorcinol. The radial growth direction of β-resorcinol is the polar axis <001> (104). We measured the growth rates on the <001> direction of both spherulites and single crystals. For spherulites growing at room temperature, the growth rate decrease is comparable for both additives since the growth rate under high undercoolings was determined by the diffusivity or viscosity of the host molecule, not interface kinetics. For single crystals, only the fast growing $+c$ direction could be measured, while the slow growing $-c$ direction was essentially immobile. We found that 2-methylresorcinol inhibited growth much more strongly compared with 5-methylresorcinol. Given that 2-methylresorcinol adsorbed more easily on $\{011\}$ facets than $\{01\bar{1}\}$ (**Figure 6**), we could assign the faster growing direction to the $+c$ direction.

We reinvestigated the interactions of L- and D-tartaric acids with facets of β-resorcinol using atomistic simulations (104). Computational results revealed an equilibrium binding constant of 15 favoring L-tartaric acid over D-tartaric acid on $(11\bar{1})$ facets, with a precisely opposite distribution for enantiomers on $(1\bar{1}\bar{1})$, indicating that tartaric acid bound enantioselectively to chiral surfaces of β-resorcinol. The enantiomers determined the sense of twist for resorcinol crystallites, but as stated above, it would be difficult to refer to tartaric acid as a TMA in the context of resorcinol. How it works is not obvious. Additionally, we had a 50% chance of choosing the correct enantiomer.

Scrutiny of the Mueller matrix micrographs of the absolute linear retardance (|LR|) of the nuclei of several twisted β-resorcinol spherulites shows a range of structures other than what was formerly observed, $+c$ growth in all radial directions (99). In **Figure 7a**, we see a roughly spherically symmetric object, indicating that the spherulite grows from a single nucleus in a common direction, in phase. A double spiral belies a twinned nucleus in **Figure 7b**. Polar spherulite growth (**Figure 7c,d**) is further discussed in the next section.

3.2.2. L-malic acid.
The greatest moment in the history of molecular chirality undeniably occurred in 1848 when Pasteur (105) separated the enantiomorphous crystals of sodium ammonium tartrate from optically inactive paratartaric acid, dissolved the respective batches, and showed that they were optically active with equal and opposite rotations of polarized light. Pasteur had
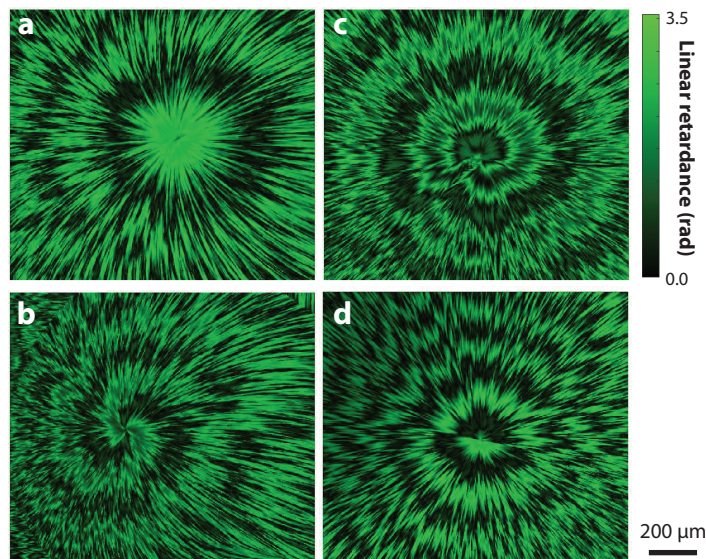
Figure 7

Linear retardance images showing a variety of the nuclei of β-resorcinol spherulites. (*a*) A spherically symmetric nucleus showing crystallites growing uniaxially in phase. (*b*) A twinned nucleus showing crystallites growing uniaxially out of phase. (*c,d*) Asymmetric nuclei showing polar spherulite growth.

correlated chirality that he could see and feel—the shapes of macroscopic crystals—with the configuration of atoms in invisible molecules. Ambition drove Pasteur to investigate deoxytartaric acid, also known as malic acid, which today we know has one less stereogenic center than tartaric acid (106). Pasteur was trying to make lightning strike twice. Of course, he did ultimately make lightning strike many times, but not in this case. Pasteur prepared racemic and L-malic acid samples and recorded their melting points by placing small amounts of powders in glass tubes next to thermometers in oil baths. He did not look at his melts in the petrographic microscope. A hot stage for a microscope was not invented until more than a generation later (107). If Pasteur had looked at a melted film between crossed polarizers, he would have noticed that recrystallized melted films formed banded spherulites at high undercoolings and likely recognized their significance (108).

As shown previously (47), and as discussed above for resorcinol, assigning the sense of a polar axis is an important function of TMAs. Malic acid crystallizes as enantiomorphs in the space group $P2_1$. The *b*-axis is the fast growth direction, and therefore its spherulites are polar. This is evident in the incomplete radial forms grown by L-malic acid from the melt, wherein one side is defined by flat edges with a brush of straight crystals emerging from the center (**Figure 8***c*). In the presence of 15 wt% L-threitol (the 2*S*,3*S* configuration), however, the growth of straight crystals was suppressed and the incomplete sphere eventually closed, forming one eye near the nucleus (**Figure 8***d*) as opposed to the typical pair (54), more similar to the case in **Figure 7***c*.

3.2.3. Aspirin. Aspirin is the ninetieth entry in Bernauer's table. He reported that it can twist from the melt when ostensibly pure (in fact, on melting, some of it is hydrolyzed to produce a TMA, salicylic acid) (87). Twisting can be mimicked by added salicylic acid, and the pitch is reduced (twisting rate increases) with increasing salicylic acid. Salicylic acid is likely a TMA for aspirin, presumably inserting itself in hydrogen bond dimers where $(-COOH)_2$ bonds are exposed. Aspirin also twists with each of his five resinous additives in *"Gedrillte" Kristalle* (20).
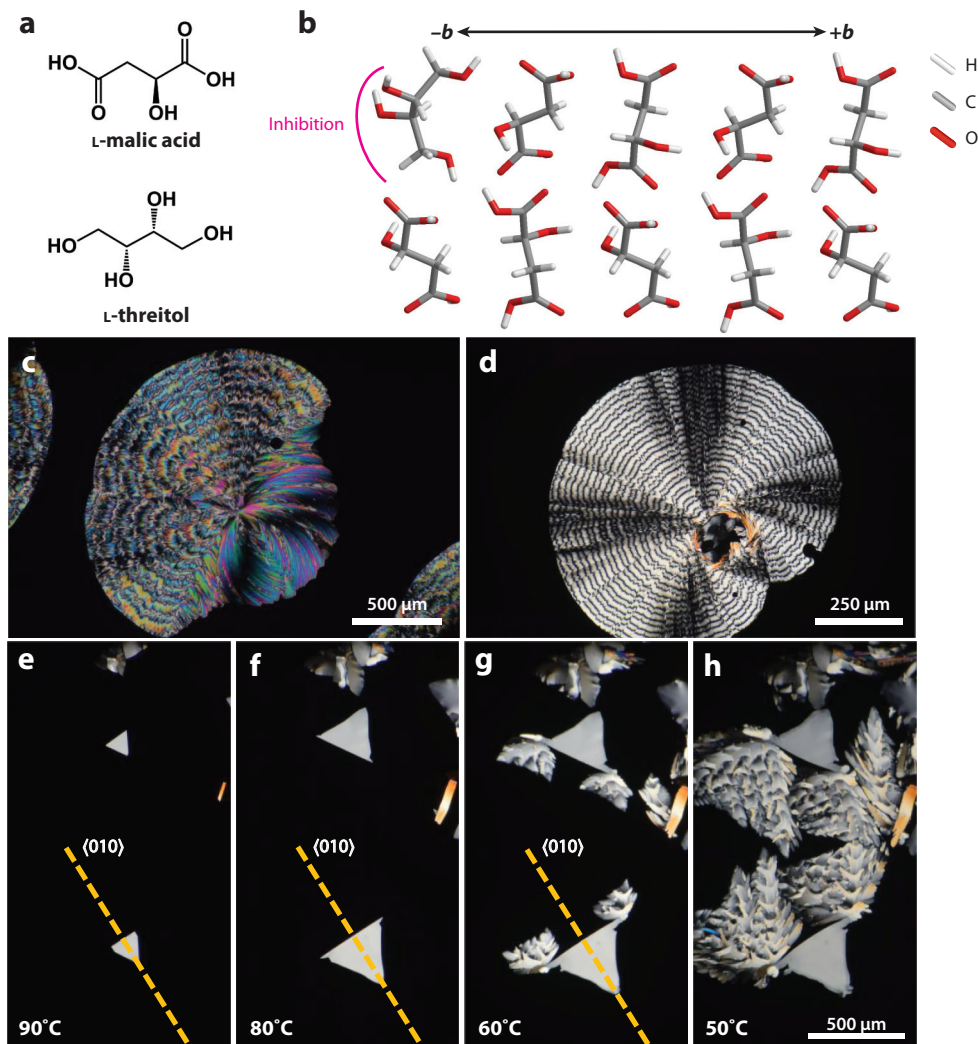
Figure 8

Growth of ʟ-malic acid from the melt. (*a*) Chemical structures of ʟ-malic acid and ʟ-threitol. (*b*) Projection of the crystal structure of ʟ-malic acid on the (100) plane, with ᴅ-tartaric acid and *meso*-tartaric acid binding preferably on (0$\bar{1}$0) and (010) planes, respectively. (*c*) Banded spherulites of pure ʟ-malic acid. (*d*) Banded spherulites of ʟ-malic acid with 15 wt% ʟ-threitol. (*e–h*) Photographs showing the effect of ʟ-threitol on ʟ-malic acid at low undercoolings. Dashed lines represent the diad axis. Panels *c–h* adapted with permission from Reference 108.

At low driving forces, aspirin single crystals grown without additives and with 9 mol% or with 19 mol% salicylic acid exhibited increasing aspect ratios (growing from approximately 15 to 30 to 45 for crystals elongated along *b* at 6° undercooling), indicating that salicylic acid presumably inhibits growth of aspirin crystallites in the orthogonal directions. Thinner aspirin lamellae from salicylic acid twisted more readily at high driving forces (30). Benzoic and *para*-aminobenzoic acids have similar effects.

Banded aspirin spherulites are remarkable enantiopolar objects. Every crystallite that branched from one end of the centric nucleus remembers in its sense of twist whether its parent (*hkl*) facet

had indices hkl or $\bar{h}\bar{k}\bar{l}$. Fields of innumerable crystallites, sometimes covering as much as a square millimeter, retain their sense and overall symmetry. Of course, symmetry is made to be broken. We added all the chiral amino acids into aspirin melts, as did Lahav, Leiserowitz, and coworkers (39, 41–47). Aspirin spherulites were always frustratingly bisected into left and right halves with occasional pathological individuals (109). We used still other chiral acids (tartaric acid, malic acid), and other chiral compounds as well, but to no avail. Heterochirality was a persistent feature of achiral aspirin.

We return here to Canada balsam, traditionally used as a glue to fix cover slips to microscope slides. It is likely that Bernauer accidentally discovered that Canada balsam, when mixed with an organic compound, has the remarkable effect of producing an optical rhythm in crystals he was trying to fix when examined between crossed polarizers. In our hands, the volatile essential oils of Canada balsam were steam distilled and characterized as additives to aspirin melt growth (110). None of the major components of the distillate—β-pinene (27%), α-pinene (26%), β-phellandrene (23%), limonene (9%), δ-3-carene (2%), and myrcene (2%)—affected the morphology of aspirin crystals grown from the melt. Among the nonvolatile components of Canada balsam are diterpenoids such as abietic acid (melting point of ∼160°C, close to that of aspirin at 135°C), the most abundant of the so-called resin acids and a very effective twisting agent for aspirin.

Schematic drawings of the symmetry breaking of the circular retardance of aspirin spherulites in the presence of chiral additives are given in **Figure 9a**. When abietic acid was mixed with
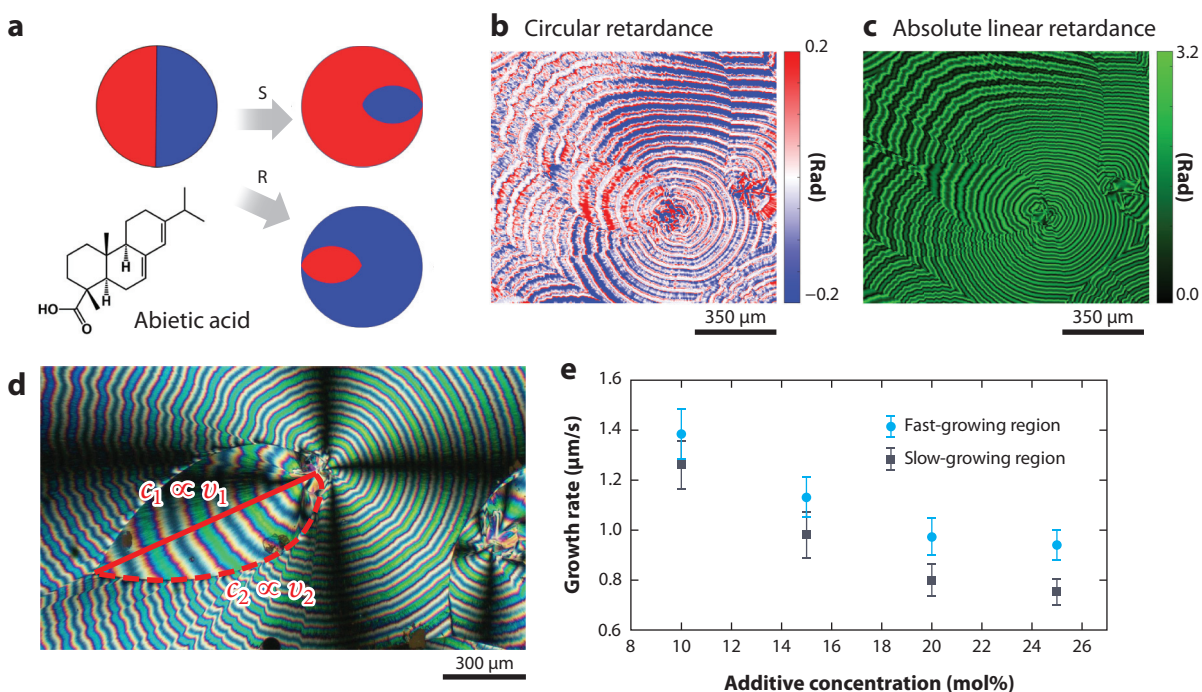

Figure 9

Aspirin grown with abietic acid. (*a*) Scheme of enantiopolar spherulite devolving into unequal, heterochiral halves in the presence of chiral additives, indicated as S and R. The chemical structure of abietic acid is also shown. (*b,c*) Circular retardance and absolute linear retardance micrograph of twisted aspirin spherulites grown with 15 mol% abietic acid. (*d*) Twisted spherulites grown with 15 mol% abietic acid including two curves illustrating the growth path of the two regions from the same nucleus. (*e*) Growth rate of two regions with different additive concentrations at 50°C.

aspirin at concentrations larger than 10 mol%, the spherulites were divided into two regions with clear grain boundaries (**Figure 9d**). The smaller leaf-like region (leaf) exhibited a larger twisting pitch and a slower growth rate compared with the larger region (outer part). Mueller matrix imaging polarimetry was applied to characterize the CR and |LR|. **Figure 9b,c** shows the CR and |LR| micrographs derived from the raw Mueller matrix. As discussed above, the optical activity of centrosymmetric aspirin was caused by the superimposition of twisted lamellae; thus, the CR of twisted aspirin was not zero. It was also established previously that right-handed aspirin crystallites show positive CR whereas left-handed helicoids show negative CR. CR oscillated in phase with LR, which is consistent with previous characterizations with salicylic acid additives (87). The leaf exhibited positive CR values and was thus comprised of right-handed helicoids, while the outer region exhibited negative CR values, indicating left-handed helicoids.

The two regions grew from the same nucleus, and the division was caused by overgrowth of the slow-growing leaf by the fast-growing outer part. In addition, since such division was driven by a growth rate difference, a model for calculating the ratio of the leaf to the outer part can be established from the growth rates of the two regions (**Figure 9e**). The calculation based on growth rates and the actual area ratio was consistent; thus, controlling the leaf area is possible by controlling the growth rate with additive concentrations and temperatures. A higher growth temperature or a larger additive concentration would further shrink the leaf. Differences in pitch for the two regions were not quantitatively studied since small leaves often lack complete pitches. Given that the leaf region grew more slowly than the outer part and that abietic acid slows growth in both regions compared with unadulterated melt, abietic acid has an extra inhibitory effect on the leaf. This was investigated computationally.

The Adsorption Locator module in Materials Studio (111) was applied to quantitatively calculate the total energy of the aspirin–abietic acid system as well as the adsorption energy of abietic acid on different {011} facets of aspirin crystals built in vacuum. The module was used to apply Monte Carlo methods to evaluate the most stable configurations of a single abietic acid molecule adsorbing on aspirin surfaces, with charges and geometries optimized based on the COMPASS force field (112). The adsorbing sites were assumed to be carboxylic groups of aspirin. Repeated simulations of cycles of 40,000 steps each were conducted to retrieve 100 configurations of the least energy for different facets. The most favorable configuration was determined to be abietic acid forming a dimer bonded by carboxylic groups with another aspirin molecule on the crystal surface. The adsorption energy of abietic acid was found to be 1.8 kJ/mol larger on (011) and ($01\bar{1}$) facets compared with ($0\bar{1}1$) and ($0\bar{1}\bar{1}$) facets, averaged over these configurations. The adsorption energy was slightly larger in the $+b$ direction. One of the H-bonds on the less-well-binding face is particularly long and bent (**Figure 10**).

Given that the abietic acid prefers to adsorb on facets along the $+b$ direction, the absolute growth direction of the aspirin spherulites can be assigned. The right-handed helicoids were growing in a more inhibited direction, so the right-handed helicoids corresponded to the $+b$, [010] direction and the fast-growing left-handed helicoids corresponded to the $-b$, [$0\bar{1}0$] direction.

4. SUMMARY AND PROSPECTS

TMAs in melts at low driving force should and do work like TMAs in solutions, although there are surprisingly few well-articulated examples. *m*-CNB stands in a class by itself as the subject of half a dozen papers (69–75). Resorcinol has been the focus of one study (99) and malic acid another (108). Aspirin also appears herein and elsewhere (87).

At high driving forces, we have a wealth of data. Let us return to **Figure 1**, an example of melt growth at large undercooling where the driving force is high and single crystals are not expected.
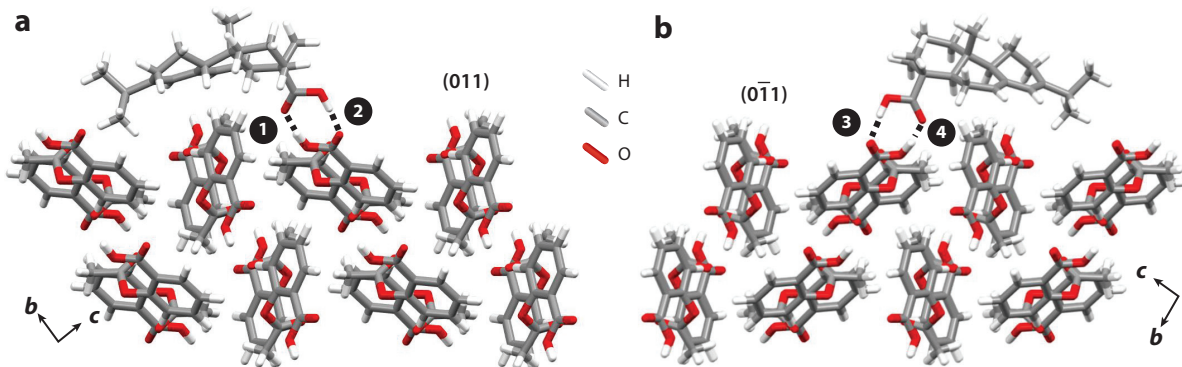
Figure 10

Adsorption of abietic acid on (011) and (0$\bar{1}$1) growth fronts of aspirin showing less stable H-bonds formed on the (0$\bar{1}$1) face due to steric hindrance. The labeled H-bonds (*black dotted lines*) have bond angles and lengths as follows: ① 167.8°, 1.70 Å; ② 166.7°, 1.70 Å; ③ 154.0°, 1.78 Å; ④ 167.8°, 1.68 Å.

Something dramatic is happening—spontaneous pattern formation—and it is additive induced. We know from our aggregate studies that it involves crystals that twist (21). Twisting of molecular crystals from the melt with or without additives is a process that is so remarkably common, and has long since been revealed to be common, that it is a wonder it has yet to become common knowledge. This now appears to be changing as more researchers are becoming attuned to seeing twisting in small molecule crystallites (113–115).

Generally speaking, twisting of molecular crystals from melts can be stereospecific, and the sense of twist can be correlated to the configuration of the molecules in the crystals, to the configuration of the molecules in the additive, to the space group of the crystals themselves, or to the dissymmetry of the growth direction in symmetric crystals.

The principal roles of resinous additives in the examples derived from "*Gedrillte" Kristalle* seem to be clear: They increase viscosities, inhibit nucleation, permit large undercoolings, increase crystallographic driving forces, and, in this way, force extreme habits. Finer crystallites typically form at higher supercooling and higher additive concentration because of more frequent branching. Finer twisted crystals, by whatever mechanism, typically have smaller pitches (21, 25, 54, 90, 116).

Small molecules working as TMAs can also reduce the crystallite cross section, as in the case of salicylic acid (87), but many other compounds can have the same effect nonspecifically. Since salicylic acid works as a sensible TMA at low driving force, we can conjecture that it is working likewise as a TMA, in part, at high driving force. It modifies the habit near the melting point and actualizes the twisting at much cooler temperatures. The same supramolecular interactions explain both results.

A motivating question for us throughout this review was whether we could find evidence for a TMA in the complex mixtures that Bernauer used to twist crystals, a TMA with the capacity to enable stereochemical assignments such as absolute structure or absolute polarity in the classic, high style we find in the citations within (see, for example, 47). We found such an additive in abietic acid, the most abundant diterpene in Canada balsam. It has the capacity to break the mirror symmetry in the fields of the CR of aspirin, something it, and thus far it alone, has done reliably; however, it is indifferent to aspirin at low driving force. Thus, when diffusion is comparatively high, it is not a very discriminating TMA. It does not seem to differentiate among the principal {*hkl*} facets. In glassy mixtures, however, when forced to interact with aspirin crystals it sufficiently

affects the growth rate along enantiopolar directions to bias the typical bisection of spherulites and to alter the twisting pitch in the fast- and slow-growing regions.

As to the mechanisms of twisting, let alone the sense and symmetry relations, it is becoming clear that in small crystals, space group symmetry is something that flexible dissymmetric molecules may endure if they want to take advantage of the thermodynamic driving force of growth, but if crystals remain slender enough, global mechanical deformations may be preferred elastically over the constraints of space group symmetry (30, 31, 117). In other words, an alternative way to express the process of molecular crystal growth is that whenever parts of an assembly (molecules in a crystal) must distort themselves to be joined together, they will inevitably be associated with geometric frustration. In fields of slender lamellae rapidly growing radially, the only mechanical deformation that is probable given space constraints is twisting around radii; however, helicoids are inconsistent with 3D lattices. If they want to continue to benefit from the chemical potential of the medium, they must straighten. This is a nontraditional view of the polyhedral world of single crystals.

It is also increasingly clear that interactions among slender crystals can promote cooperative twisting or braiding (117, 118). Lattice mismatch between intimately but intergrown layers of fibers may lead to surface forces that, in turn, twist the composites. A shear can arise at crystallographically misoriented lamellae with strain in proportion to a misorientation angle, although these ideas are not restricted to crystallographic bi- and multilayered structures (119–121). Grason (122) has explored in detail the elastic consequences of twisting bundles of parallel fibers that are abundant in many biologic, polymeric, and liquid crystalline architectures. The intersection between this work and what is described herein is likely more substantial than known so far.

DISCLOSURE STATEMENT

The authors are not aware of any affiliations, memberships, funding, or financial holdings that might be perceived as affecting the objectivity of this review.

ACKNOWLEDGMENTS

LITERATURE CITED

1. Ulrich J, Nyvlt J. 2008. *Admixtures in Crystallization*. New York: Wiley
2. Buckley HE. 1951. *Crystal Growth*. New York: Wiley
3. Sangwal K. 2007. *Additives and Crystallization Processes: From Fundamentals to Applications*. New York: Wiley
4. Kelley MP, Chow JK, Kahr B. 1994. Critical evaluation of dyes and crystal growth inhibitors. *Mol. Cryst. Liq. Cryst.* 242:201–14
5. Buckley HE. 1933. Systematic habit-variation in $KClO_3$ crystals produced by dyes. *Z. Krist.* 85:58–73
6. Buckley HE. 1934. Molecular configuration and its relation to modification of crystal-growth. *Z. Krist.* 88:381–410
7. Buckley HE. 1938–1939. Some problems connected with crystal-growth. *Mem. Proc. Manch. Lit. Philos. Soc.* 83:31–46
8. Buckley HE. 1951. Studies in the growth and habit modification of crystals. *Mem. Proc. Manch. Lit. Philos. Soc.* 88:381–410
9. Kahr B, Gurney RW. 2001. Dyeing crystals. *Chem. Rev.* 101:893–951
10. Kahr B, Kelley MP. 1995. Diastereospecific recognition of dyes by salt crystals: a case of plundered stereochemistry in postwar Europe. In *Supramolecular Stereochemistry*, ed. JS Siegel, pp. 203–27. Dordrecht, Neth.: Kluwer

11. Kelley MP, Janssens B, Vetter W, Kahr B. 1994. Recognition of dyes by K_2SO_4 surfaces: choosing organic guests for simple salts. *J. Am. Chem. Soc.* 116:5519–20

12. Gurney RW, Mitchell CA, Ham S, Bastin LD, Kahr B. 2000. Salting benzenes. *J. Phys. Chem. B* 104:878–92

13. Kahr B, Shtukenberg AG. 2016. Dyeing crystals since 2000. *CrystEngComm* 18:8988–98

14. Kaminsky W, Claborn K, Kahr B. 2004. Polarimetric imaging of crystals. *Chem. Soc. Rev.* 33:514–25

15. Claborn K, Chu A-S, Jang S-H, Su F, Kaminsky W, Kahr B. 2005. Circular extinction imaging: determination of the absolute orientation of embedded chromophores in enantiomorphously twinned $LiKSO_4$ crystals. *Cryst. Growth Des.* 5:2117–23

16. Benedict JB, Cohen D, Lovell S, Rohl A, Kahr B. 2006. What is syncrystallization? States of the pH indicator methyl red in crystals of phthalic acid. *J. Am. Chem. Soc.* 128:5548–59

17. Wustholz KL, Bott ED, Isborn CM, Li X, Kahr B, Reid PJ. 2007. Dispersive kinetics from single molecules oriented in single crystals of potassium acid phthalate. *J. Phys. Chem. C* 111:9146–56

18. Wustholz KL, Kahr B, Reid PJ. 2005. Single-molecule orientations in dyed salt crystals. *J. Phys. Chem. B* 109:16357–62

19. Bernauer F. 1927. Über Zickzackbänderung (Runzelbänderung) und verwandte Polarisationserscheinungen an Kristallen und Kristallaggregaten. *N. Jahrb. Mineral. Geol. Paleont.* 55:92–143

20. Bernauer F. 1929. *"Gedrillte" Kristalle*. Berlin: Gebrüder Borntraeger

21. Shtukenberg AG, Punin YO, Gujral A, Kahr B. 2014. Growth actuated bending and twisting of single crystals. *Angew. Chem. Int. Ed.* 53:672–99

22. Kahr B, Shtukenberg AG. 2017. Seeing molecular configuration in twisted crystal form. *Isr. J. Chem.* 57:31–8

23. Ball P. 2001. *The Self-Made Tapestry: Pattern Formation in Nature*. Oxford, UK: Oxford Univ. Press

24. Shtukenberg AG, Gunn E, Gazzano M, Freudenthal J, Camp E, et al. 2011. Bernauer's bands. *Chem. Phys. Chem.* 12:1558–71

25. Shtukenberg AG, Yang Y, Zhu X, Kahr B. 2020. Common occurrence of twisted molecular crystal morphologies from the melt. *Cryst. Growth Des.* 20:6186–97

26. Kahr B, Tan M, Ye H-M, Shtukenberg AG. 2019. Polymorphism and morphology folklore. *Cryst. Growth Des.* 19:5999–6003

27. Yang Y, Shtukenberg AG, Sun M, Hu CT, Lee S, Kahr B. 2022. Transport in twisted crystalline charge transfer complexes. *Chem. Mater.* 34:1778–88

28. Crist B, Schultz JM. 2016. Polymer spherulites: a critical review. *Prog. Polym. Sci.* 56:1–63

29. Lovinger A. 2020. Twisted crystals and the origin of banding in spherulites of semiconducting polymers. *Macromolecules* 53:741–45

30. Haddad A, Aharoni H, Sharon E, Shtukenberg AG, Kahr B, Efrati E. 2019. Twist renormalization in molecular crystals driven by geometric frustration. *Soft Matter* 15:116–26

31. Li C, Shtukenberg AG, Vogt-Maranto L, Efrati E, Raiteri P, et al. 2020. Why are some crystals straight? *J. Phys. Chem. C* 124:15616–24

32. Zhang Y, Shtukenberg AG, Kahr B, Kaylyon DM, Lee SS. 2023. Effect of melt shearing on D-mannitol crystal twisting in the presence of small molecule and macromolecular additives. *J. Cryst. Growth* 601:126942

33. Dandekar P, Kuvadia ZB, Doherty MF. 2013. Engineering crystal morphology. *Annu. Rev. Mater. Res.* 43:359–86

34. Shtukenberg AG, Lee SS, Kahr B, Ward MD. 2014. Manipulating crystallization with molecular additives. *Annu. Rev. Chem. Biomol. Eng.* 5:77–96

35. Lovette MA, Browning AR, Griffin DW, Sizemore JP, Snyder RC, et al. 2008. Crystal shape engineering. *Ind. Eng. Chem. Res.* 47:9812–33

36. De Yoreo JJ, Vekilov PG. 2003. Principles of crystal nucleation and growth. *Rev. Mineral. Geochem.* 54:57–93

37. Sunagawa I. 2007. *Crystals: Growth, Morphology, and Perfection*. Cambridge, UK: Cambridge Univ. Press

38. Chernov AA. 1984. *Modern Crystallography III. Crystal Growth*. Berlin: Springer

39. Berkovitch-Yellin Z, Van Mil J, Addadi L, Idelson M, Lahav M, et al. 1985. Crystal morphology engineering by "tailor-made" inhibitors; a new probe to fine intermolecular interactions. *J. Am. Chem. Soc.* 107:3111–22

40. Engwerda AHJ, van Schayik P, Jagtenberg H, Meekes H, Rutjes FPJT, Vlieg E. 2018. Deracemization of a racemic compound by using tailor-made additives. *Chem. Eur. J.* 24:2863–67

41. Addadi L, van Mil J, Gati E, Lahav M. 1981. Amplification of optical activity by crystallization in the presence of tailor-made additives. The "inversion rule." *Orig. Life* 11:355–64

42. Addadi L, Berkovitch-Yellin Z, Weissbuch I, Lahav M, Leiserowitz L, et al. 1982. Use of "enantiopolar" directions in centrosymmetric crystals for direct assignment of absolute configuration of chiral molecules: application to the system serine/threonine. *J. Am. Chem. Soc.* 104:2075–77

43. Shimon LJW, Lahav M, Leiserowitz L. 1985. Design of stereoselective etchants for organic crystals. Application for the sorting of enantiomorphs and direct assignment of absolute configuration of chiral molecules. *J. Am. Chem. Soc.* 107:3375–77

44. Weissbuch I, Popovitz-Biro R, Lahav M, Leiserowitz L. 1995. Understanding and control of nucleation, growth, habit, dissolution and structure of two- and three-dimensional crystals using 'tailor-made' auxiliaries. *Acta Crystallogr. B* 51:115–48

45. Lahav M, Addadi L, Leiserowitz L. 1987. Chemistry at the surfaces of organic crystals. *PNAS* 84:4737–38

46. Weissbuch I, Addadi L, Lahav M, Leiserowitz L. 1991. Molecular recognition at crystal interfaces. *Science* 253:637–45

47. Addadi L, Berkovitch-Yellin Z, Weissbuch I, Lahav M, Leiserowitz L. 1986. A link between macroscopic phenomena and molecular chirality: crystals as probes for the direct assignment of absolute configuration of chiral molecules. In *Topics in Stereochemistry*, Vol. 16, ed. EL Eliel, SH Wilen, NL Allinger, pp. 1–85. New York: Wiley

48. Rimer JD, An Z, Zhu Z, Lee MH, Goldfarb DS, et al. 2010. Crystal growth inhibitors for the prevention of L-cystine kidney stones through molecular design. *Science* 330:337–41

49. Shtukenberg AG, Poloni LN, Zhu Z, An Z, Bhandari M, et al. 2015. Dislocation-actuated growth and inhibition of hexagonal L-cystine crystallization at the molecular level. *Cryst. Growth Des.* 15:921–34

50. Poloni LN, Zhu Z, Garcia-Vázquez N, Yu AC, Connors DM, et al. 2017. Role of molecular recognition in L-cystine crystal growth inhibition. *Cryst. Growth Des.* 17:2767–81

51. Shtukenberg AG, Hu L, Sahota A, Kahr B, Ward MD. 2022. Disrupting crystal growth through molecular recognition: designer therapies for kidney stone prevention. *Acc. Chem. Res.* 55:516–25

52. Yang Y, Albanyan H, Lee S, Aloysius H, Liang J-J, et al. 2018. Design, synthesis, and evaluation of L-cystine diamides as L-cystine crystallization inhibitors for cystinuria. *Bioorg. Med. Chem. Lett.* 28:1303–8

53. Klapper H. 2010. Generation and propagation of defects during crystal growth. In *Springer Handbook of Crystal Growth*, ed. G Dhanaraj, K Byrappa, V Prasad, M Dudley, pp. 93–132. Heidelberg, Ger.: Springer

54. Shtukenberg AG, Punin Y-O, Gunn E, Kahr B. 2012. Spherulites. *Chem. Rev.* 112:1805–38

55. Jackson KA, Uhlmann DR, Hunt JD. 1967. On the nature of crystal growth from the melt. *J. Cryst. Growth* 1:1–36

56. Perepezko JH. 1997. Kinetic processes in undercooled melts. *Mater. Sci. Eng. A* 226–228:374–82

57. Jia S, Gao Z, Tian N, Li Z, Gong J, et al. 2021. Review of melt crystallization in the pharmaceutical field, towards crystal engineering and continuous process development. *Chem. Eng. Res. Des.* 166:268–80

58. Veintemillas-Verdaguer S. 1996. Chemical aspects of the effect of impurities in crystal growth. *Prog. Cryst. Growth Charact. Mater.* 32:75–109

59. Parks GS, Spaght ME, Barton LE. 1935. Viscosity data for commercial rosin and abietic acid. *Ind. Eng. Chem. Res.* 7:115–16

60. Shtukenberg AG, Ward MD, Kahr B. 2022. Crystal growth inhibition by impurity stoppers, now. *J. Cryst. Growth* 597:126839

61. Kahr B, Shtukenberg AG, Yang J, Ward MD. 2021. Tailor-made additives for polar growth from melts. *Isr. J. Chem.* 61:583–89

62. Olijve LLC, Meister K, DeVries AL, Duman JG, Guo S, et al. 2016. Blocking rapid ice crystal growth through nonbasal plane adsorption of antifreeze proteins. *PNAS* 113:3740–45

63. Harding MM, Ward LG, Haymet ADJ. 1999. Type I 'antifreeze' proteins. *Eur. J. Biochem.* 264:653–65

64. Damodaran S. 2007. Inhibition of ice crystal growth in ice cream mix by gelatin hydrolysate. *J. Agric. Food Chem.* 55:10918–23

65. Feeney RE, Yeh Y. 1998. Antifreeze proteins: Current status and possible food uses. *Trends Food Sci. Technol.* 9:102–6

66. Shtukenberg AG, Ward MD, Kahr B. 2017. Crystal growth with macromolecular additives. *Chem. Rev.* 117:14042–90

67. Drori R, Li C, Hu C, Raiteri P, Rohl AL, et al. 2016. A supramolecular ice growth inhibitor. *J. Am. Chem. Soc.* 138:13396–401

68. Carenco A, Jerphagnon J, Perigaud A. 1977. Nonlinear optical properties of some *m*-disubstituted benzene derivatives. *J. Chem. Phys.* 66:3806–13

69. Murata Y, Honda T. 1977. The growth of *m*-chloronitrobenzene crystals. *J. Cryst. Growth* 39:315–27

70. Matsuoka M, Garside J, Rout JE, Black SN, Davey RJ. 1990. The influence of melt composition on the crystal morphology of *m*-chloronitrobenzene. *J. Cryst. Growth* 99:1138–41

71. Chen BD, Garside J. 1991. A comparison of the morphology of m-chloronitrobenzene crystals grown from solution and from the melt. *J. Phys. D. Appl. Phys.* 24:131–34

72. Chen B, Garside J, Davey RJ, Maginn SJ, Matsuoka M. 1994. Growth of *m*-chloronitrobenzene crystals in the presence of tailor-made additives: assignment of the polar axes from morphological calculations. *J. Phys. Chem.* 98:3215–21

73. Chen B, Potts GD, Davey RJ, Garside J, Bergmann D, et. al. 1994. Growth of meta-chloronitrobenzene crystals in the presence of "tailor-made" additives: assignment of the polar axes from morphological changes. *J. Cryst. Growth* 144:297–303

74. Takiyama H, Okada Y, Arita H, Uchida H, Matsuoka M. 2002. Morphological changes and local purities of m-CNB crystals. *J. Cryst. Growth* 235:494–98

75. Funakoshi K. 2018. Melting inhibition behaviors of *m*-chloronitrobenzene crystals by addition of *p*-chloronitrobenzene. *J. Chem. Eng. Jpn.* 51:625–30

76. Docherty R, Roberts KJ. 1988. Modelling the morphology of molecular crystals; application to anthracene, biphenyl and β-succinic acid. *J. Cryst. Growth* 88:159–68

77. Gránásy L, Pusztai T, Börzsönyi T, Tóth GI, Tegze G, et al. 2006. Polycrystalline patterns in far-from-equilibrium freezing: a phase field study. *Philos. Mag.* 86:3757–78

78. Boys SF. 1934. Optical rotatory power. I—a theoretical calculation for a molecule containing only isotropic refractive centres. *Proc. R. Soc. A* 144:655–75

79. Devarajan V, Glazer AM. 1986. Computation of optical rotatory power in inorganic crystals. *Acta Crystallogr. A.* 42:560–69

80. Gunn E, Sours R, Benedict JB, Kahr B. 2006. Mesoscale chiroptics of rhythmic precipitates. *J. Am. Chem. Soc.* 128:14234–35

81. Freudenthal J, Kahr B. 2008. Dendritic crystal growth, asymmetric photochemistry, and the origin of biomolecular homochirality. *Chirality* 20:973–77

82. Tan M, Jiang W, Martin AT, Shtukenberg AG, McKee MD, Kahr B. 2020. Polarized light through polycrystalline vaterite helicoids. *Chem. Commun.* 56:7353–56

83. Helmbrecht L, Tan M, Röhrich R, Bistervels MH, Kessels BO, et al. 2019. Directed emission from self-assembled microhelices. *Adv. Funct. Mater.* 30:1908218

84. Ye H-M, Tan M, Freudenthal JF, Kahr B. 2019. Chiroptical differentiation of twisted chiral and achiral polymer crystals. *Macromolecules* 2:8514–20

85. Yang Y, Zong K, Whittaker SJ, An Z, Tan M, et al. 2022. Twisted tetrathiafulvalene crystals. *Mol. Syst. Des. Eng.* 7:569–76

86. Yang Y, de Moraes LS, Ruzié C, Schweicher G, Geerts YH, et al. 2022. Charge transport in twisted organic semiconductor crystals of modulated pitch. *Adv. Mater.* 34:2203842

87. Cui X, Rohl AL, Shtukenberg A, Kahr B. 2013. Twisted aspirin crystals. *J. Am. Chem. Soc.* 135:3395–98

88. Martin AT, Nichols SM, Murphy VL, Kahr B. 2021. Chiroptical anisotropy of crystals and molecules. *Chem. Commun.* 57:8107–20

89. Arteaga OB, Kahr B. 2019. Mueller matrix polarimetry of bianisotropic materials. *J. Opt. Soc. Am. B* 36:F72–83

90. Cui X, Shtukenberg AG, Freudenthal J, Nichols S, Kahr B. 2014. Circular birefringence of banded spherulites. *J. Am. Chem. Soc.* 136:5481–90

91. Shtukenberg AG, Cui X, Freudenthal J, Gunn E, Camp E, et al. 2012. Twisted mannitol crystals establish homologous growth mechanisms for high-polymer and small-molecule ring-banded spherulites. *J. Am. Chem. Soc.* 134:6354–64

92. Cui X, Nichols SM, Arteaga O, Freudenthal J, Paula F, et al. 2016. Dichroism in helicoidal crystals. *J. Am. Chem. Soc.* 138:12211–18

93. Kaminsky W. 2000. Experimental and phenomenological aspects of circular birefringence and related phenomena in transparent crystals. *Rep. Prog. Phys.* 63:1575–640

94. Wallerant MF. 1907. Sur les enroulements hélicoïdaux dans les corps cristallisés. *Bull. Minéral. Soc. Fr.* 30:43–60

95. Shtukenberg AG, Freudenthal J, Kahr B. 2010. Reversible twisting during helical hippuric acid crystal growth. *J. Am. Chem. Soc.* 132:9341–49

96. Ubbelohde AR, Robertson JM. 1937. A new form of resorcinol. *Nature* 140:239

97. Robertson JM, Ubbelohde AR. 1938. A new form of resorcinol. I. Structure determination by X-rays. *Proc. R. Soc. A* 167:122–35

98. Robertson JM, Ubbelohde AR. 1938. A new form of resorcinol. II. Thermodynamic properties in relation to structure. *Proc. R. Soc. A* 167:136–47

99. Zhu Q, Shtukenberg AG, Carter DJ, Yu T-Q, Yang J, et al. 2016. Resorcinol crystallization from the melt: a new ambient phase and new "riddles." *J. Am. Chem. Soc.* 138:4881–89

100. Wells AF. 1949. Abnormal and modified crystal growth. *Discuss. Faraday Soc.* 5:197–201

101. Weissbuch I, Leiserowitz L, Lahav M. 2006. Self-poisoning at {011} faces of α-resorcinol crystals may explain its unidirectional growth in the vapor phase: a molecular modeling study. *Cryst. Growth Des.* 6:625–28

102. Lahav M, Leiserowitz L. 2001. The effect of solvent on crystal growth and morphology. *Chem. Eng. Sci.* 56:2245–53

103. Lahav M, Leiserowitz L. 2006. A stereochemical approach that demonstrates the effect of solvent on the growth of polar crystals: a perspective. *Cryst. Growth Des.* 6:619–24

104. Kahr B, Shtukenberg A, Gunn E, Carter DJ, Rohl AL. 2011. Controlling mesoscale crystal helicity with additives, again. *Cryst. Growth Des.* 11:2070–73

105. Pasteur L. 1848. Mémoire sur la relation qui peut exister entre la forme cristalline et la composition chimique, et sur la cause de la polarization rotatoire. *C. R. Acad. Sci. Paris* 26:535–39

106. Pasteur L. 1852. Mémoire sur les acides aspartique et malique. *Ann. Chim. Phys.* 34:30–64

107. Lehmann O. 1888. *Molekularphysik*. Leipzig, Ger.: Engelmann

108. Yang J, Hu CT, Shtukenberg AG, Yin Q, Kahr B. 2018. ʟ-malic acid crystallization: polymorphism, semi-spherulites, twisting, and polarity. *CrystEngComm* 20:1383–89

109. Cui X. 2015. *Optical analysis of crystal twisting in banded spherulites*. PhD Diss., New York Univ., New York

110. Ross J, Gagnon H, Girard D, Hachey J-M. 1996. Chemical composition of the bark oil of balsam fir *Abies balsamea* (L.) Mill. *J. Essent. Oil Res.* 8:343–46

111. Akkermans RLC, Spenley NA, Robertson SH. 2013. Monte Carlo methods in Materials Studio. *Mol. Simul.* 39:1153–64

112. Sun H. 1998. COMPASS: an ab initio force-field optimized for condensed-phase applications – overview with details on alkane and benzene compounds. *J. Phys. Chem. B* 102:7338–64

113. Killalea CE, Amabilino DB. 2021. Stereochemistry and twisted crystals. *Isr. J. Chem.* 61:629–44

114. Polyzois H, Guo R, Srirambhatla VK, Warzecha M, Prasad E, et al. 2022. Crystal structure and twisted aggregates of oxcarbazepine form III. *Cryst. Growth Des.* 22:4146–56

115. Scheurle PI, Mähringer A, Haug T, Biewald A, Axthammer D, et al. 2022. Helical anthracene–ethyne-based MOF-74 analogue. *Cryst. Growth Des.* 22:2849–53

116. Shtukenberg AG, Gujral A, Rosseeva E, Cui X, Kahr B. 2015. Mechanics of twisted hippuric acid crystals untwisting as they grow. *CrystEngComm* 17:8817–84

117. Efrati E. 2020. Geometric frustration in molecular crystals. *Isr. J. Chem.* 60:1185–89

118. Shtukenberg AG, Drori R, Sturm E, Vidavsky N, Haddad A, et al. 2020. Crystals of benzamide, the first polymorphous molecular compound, are helicoidal. *Angew. Chem. Int. Ed.* 59:14593–601

119. Armon S, Efrati E, Kupferman R, Sharon E. 2011. Geometry and mechanics in the opening of chiral seed pods. *Science* 333:1726–30
120. Armon S, Aharoni H, Moshe M, Sharon E. 2014. Shape selection in chiral ribbons: from seed pods to supramolecular assemblies. *Soft Matter* 10:2733–40
121. Zhang M, Grossman D, Danino D, Sharon E. 2019. Shape and fluctuations of frustrated self-assembled nano ribbons. *Nat. Commun.* 10:3565
122. Grason GM. 2020. Chiral and achiral mechanisms of self-limiting assembly of twisted bundles. *Soft Matter* 16:1102–6